THE ASTROPHYSICAL JOURNAL, 220:643–665, 1978 March 1

DYNAMICS OF THE QUIESCENT SOLAR CORONA

R. ROSNER AND W. H. TUCKER
Center for Astrophysics, Harvard College Observatory and Smithsonian Astrophysical Observatory
AND
G. S. VAIANA
Center for Astrophysics, Harvard College Observatory and Smithsonian Astrophysical Observatory;
and
Osservatorio Astronomico di Palermo, Italy
Received 1977 June 8; accepted 1977 August 31

ABSTRACT

A model for the quiescent, inhomogeneous solar corona is developed, based upon the concept of loop structures as the basic structural element of the corona. The results, which are compared with observations obtained by the S-054 *Skylab* X-ray telescope, show that (*a*) hydrostatic solutions are stable only if the temperature maximum is located at the top of loop structures, and the deposition scale length of the coronal heating mechanism is comparable with (or larger than) the loop scale size; (*b*) the loop temperature ($\sim T_{\max}$), pressure p, and size L are related by the expression $T_{\max} \sim 1.4 \times 10^3 (pL)^{1/3}$, a relation which contains no free parameters; (*c*) coronal heating models based upon the coronal magnetic field (e.g., Alfvén mode dissipation and coronal current heating) are consistent with the loop model, while acoustic mode damping is not.

In accordance with these results, we propose a new model of the corona in which the quiescent X-ray corona represents a metastable equilibrium state. Thus, fluctuations in the local heating rate are shown to lead to dynamically unstable states within loops. These may be identified with transient loop brightenings seen in X-rays; with relatively cool coronal loop structures seen in EUV emission lines, which have been reported to extend to heights larger than the imputed pressure scale height and may be associated with downflows of plasma; and with the formation of quiescent prominences within loop structures.

Subject headings: Sun: corona — Sun: X-rays

I. INTRODUCTION

The conventional view regarding stellar chromospheres and coronae, particularly of late-type stars such as the Sun, is that they are by-products of convective flows in the stars' outer layers; the acoustic noise generated by these motions is thought to couple to the tenuous extended atmosphere, raising its temperature above the effective temperature of the star by virtue of the gases' relatively low radiative efficiency (see Athay 1976 and references cited therein). This traditional view has led to a large number of theoretical efforts to model observations of chromospheres and coronae, whose common element is a spatially homogeneous ("plane-parallel") description of the atmosphere (see, for example, De Loore 1970; Moore and Fung 1972; Landini and Fossi 1973; McWhirter *et al.* 1975; Jordan 1976; Vanbeveren and De Loore 1976). This approach is to some extent made inevitable by the underlying assumption of coronal heating via the dissipation of acoustic modes, because turbulent convection and the associated mode generation are thought to be fairly homogeneous over the surface of the star.

On the other hand, the early X-ray studies of the Sun carried out by rocket-borne instruments (cf. Vaiana *et al.* 1968; Van Speybroeck, Krieger, and Vaiana 1970) as well as the high-resolution data obtained by the EUV and X-ray instruments on board *Skylab* (Reeves *et al.* 1976; Tousey *et al.* 1973; Vaiana *et al.* 1973; Underwood *et al.* 1976) have shown the corona to be composed of a variety of complex looplike systems generally associated with underlying photospheric and chromospheric structures, in particular magnetic field structures. A comparison of X-ray loop structures with potential field extrapolations of the photospheric magnetic field suggests that these loops outline the three-dimensional configuration of the coronal magnetic field (Van Speybroeck, Krieger, and Vaiana 1970; Krieger, Vaiana, and Van Speybroeck 1971; Poletto *et al.* 1975).

The intensity of the X-ray emission seems also to be directly related to the magnetic field configuration; thus strong X-ray emission is found in the neighborhood of large field complexity (Krieger, Vaiana, and Van Speybroeck 1971; Poletto *et al.* 1975; McIntosh *et al.* 1976), while the regions of weakest coronal X-ray emission overlie photospheric regions devoid of magnetic activity, with one polarity generally dominant (Timothy, Krieger, and Vaiana 1975). These observations support the view that coronal radiative emission derives predominantly from plasma confined by topologically closed magnetic field structures (Pneuman 1973). The association of extremely weak

coronal emission with open-field topologies in solar coronal holes (Timothy, Krieger, and Vaiana 1975) suggests in fact that strong stellar coronae can exist only in the presence of stellar magnetic fields; the presence of convection is then only a necessary, but not sufficient, condition for the existence of a strong corona unless one can demonstrate that magnetic fields are an inevitable result of convective activity.

We conclude that, at least in the Sun's case, there is no one corona but rather many small-scale "coronae" of differing temperature and pressure which can coexist, the magnetic field providing the required "isolation." This may in fact be an advantage since instead of confronting a single corona, one confronts many; and it may therefore be possible to take advantage of systematic trends of the variation of temperature with pressure, for example, to distinguish between proposed mechanisms for heating the outer layer of the Sun and other stars.

In this paper we consider the steady-state energetics of a simple model for coronal loops. The observed morphology leads us to assume that the loop is the basic building block of all coronal features. It is assumed that the coronal temperature and density structuring is dominated by transport processes along the magnetic field in order to permit one-dimensional modeling. By emphasizing an analytical rather than a numerical approach, we seek to establish explicit relationships which show how the conditions in the loop depend upon the assumed energy deposition function and the size of the loop, and thereby to set up a useful framework for comparing observations with theory.

The loops considered in this paper are quasi-static, although gradual evolutionary changes will be considered; dynamic effects will be discussed in more detail in later papers. Our work differs from previous efforts of modeling the inner corona principally in our effort to account for the coronal X-ray observations. Our analytical approach follows initially along the lines devised by Landini and Fossi (1975), who derived a sequence of models for the X-ray corona under the assumption of spatially uniform acoustic heating, but diverges from their work in our examination of the effects of modifying the assumed heating function, our emphasis upon the closed topology of coronal structures, and our study of the consequences of locating the position of the temperature maximum within these structures.

In § II we discuss some general features of coronal loops which follow from the X-ray observations; in § III we present a simple model for coronal loops, together with a detailed discussion of the assumption involved, and in § IV we illustrate how the model may be used to gain insight into the mechanism responsible for coronal loop heating.

II. GENERAL FEATURES OF CORONAL LOOP STRUCTURES

The structure of the X-ray corona, from both morphological and quantitative points of view, has been reviewed several times (cf. Vaiana *et al.* 1976 and references cited therein); our intention here is not to repeat this material but rather to briefly summarize the available data which are immediately relevant to the construction of theoretical models.

a) *The X-ray corona is structured.* We first wish to reemphasize the view long expressed by solar X-ray observers and others that loop structures are the significant structural element of the solar corona (cf. early references such as Reidy *et al.* 1968 and Van Speybroeck, Krieger, and Vaiana 1970, as well as Dunn 1971, who reviews early non–X-ray work). Figure 1 displays some of the basic structural archetypes evident in the X-ray corona: active regions and their associated loop arcades, and large-scale structures reminiscent of the "quiet corona"; a succinct review of these and other morphological classes is found in Vaiana *et al.* (1976). In particular, we call attention to the fact that regions appearing to be unstructured in a given X-ray picture can generally be made to reveal their structuring by examining images taken either with a different filter inserted into the optical path or with the same filter but different exposure time; an example is provided in Figure 2.

For certain structures, such as bright points, this process may not be possible because of limitations imposed by the resolution of the X-ray telescope; the significant fact remains, however, that for scales larger than that defined by the telescope resolution, coronal structuring into loops can invariably be demonstrated. Further, the progressive improvements of X-ray telescope resolution achieved since the early rocket flights have shown that diffuse regions at the limit of resolution again invariably reveal loop structuring when viewed with an instrument of higher resolving power; examples of this may be found in Vaiana, Krieger, and Timothy (1973). It is therefore our contention that the corona must be identified with these structures; there is no evidence in our data to support the view that coronal loops are merely embedded in a more diffuse, unstructured background plasma.

b) *Plasma energy densities are correlated with the size and age of emitting structures.* The telescope design, which incorporated a filter wheel in the optical path, allows information beyond the purely morphological to be obtained (cf. Reidy *et al.* 1968; Vaiana, Krieger, and Timothy 1973). The most easily derived information concerns the energy density of the coronal plasma. As discussed by Landini *et al.* (1975), and in detail by Kahler (1976), one of the filter positions (filter 3) resulted in exposures for which the energy deposited on film was directly proportional to the integrated energy density $\int dlN_eT_e$ of the emitting plasma over a wide range of line-of-sight plasma temperatures; in such images, brightness is therefore directly related to the total plasma energy density in the line of sight. This fact yields two important results for the X-ray corona: first, that coronal plasma energy densities are inversely correlated with the typical size scale of the emitting regions; second, that the energy density is also inversely correlated with the age of the emitting structure. The qualitative correctness of these assertions is seen, for example, in Figure 3, which contains images taken in the filter 3 position. This figure illustrates the evolving structure of a

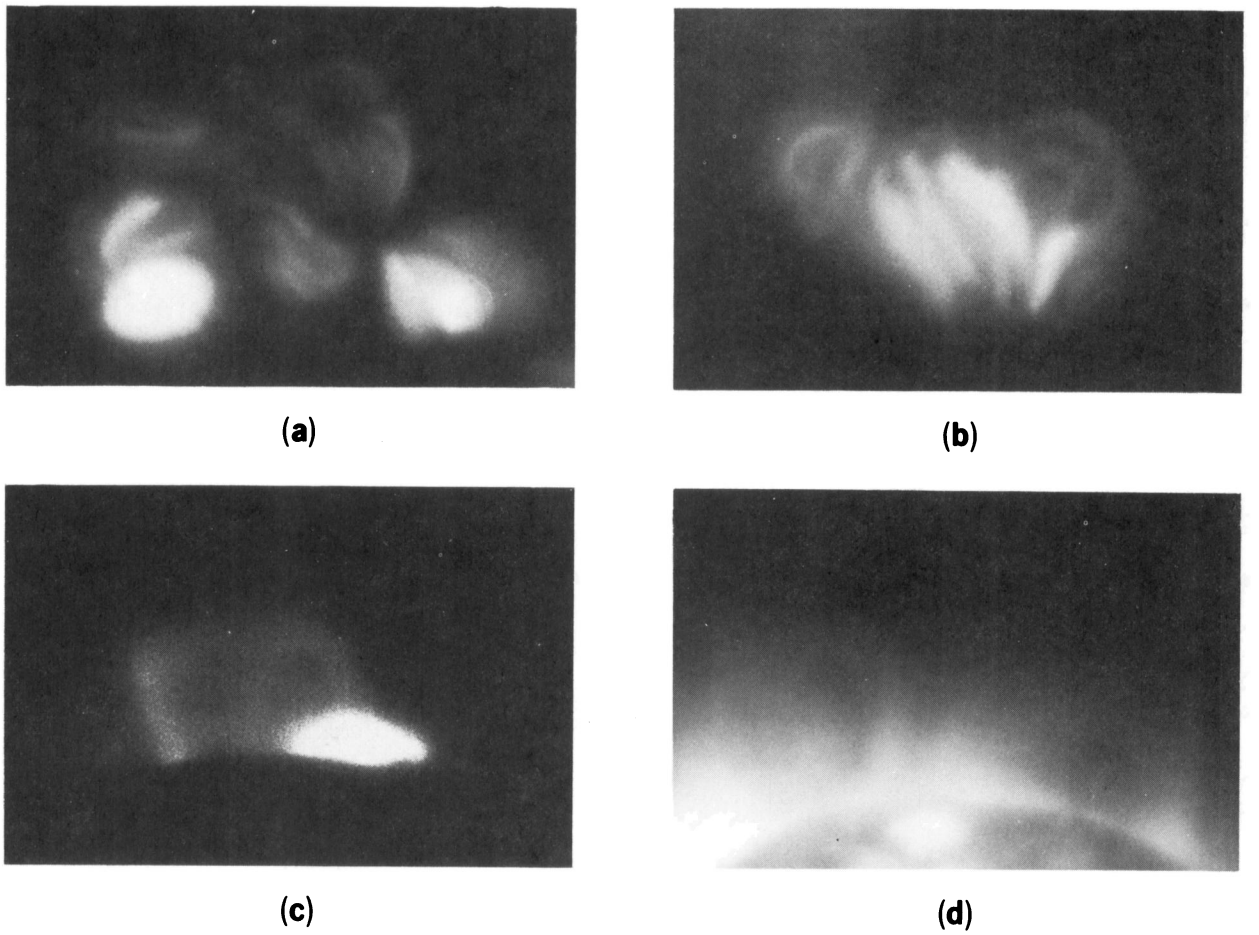

FIG. 1.—Loop structuring in the X-ray corona. Four examples of looplike structures in a range of coronal environments: (*a*) young, emerging active region complex; (*b*) well-developed active region; (*c*) postflare loops at limb; (*d*) large-scale loop structures in the "quiet Sun."

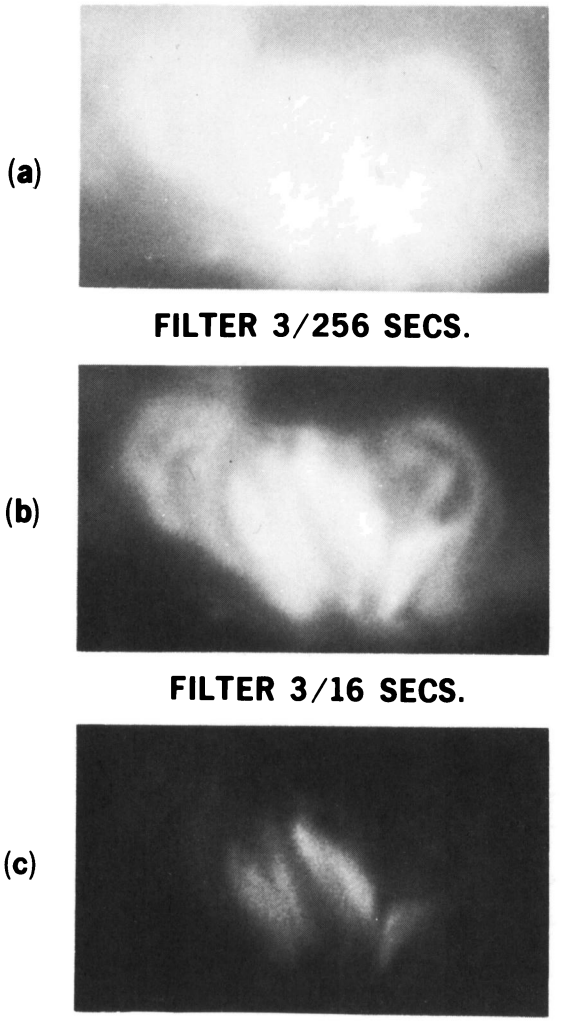

FIG. 2.—The X-ray corona is always structured. The wide dynamic range of coronal emission and the relatively narrow dynamic response of the recording medium (film) necessitates a careful choice of both filter and exposure time to reveal loop structuring in the corona. Shown are (*a*) an overexposed image, as well as (*b*) and (*c*) images taken within the dynamic limits of the film, all of the same active region.

FIG. 3.—The long-term evolution (three rotations) of an active region. Active regions begin as compact, bright loop complexes (*left*) and subsequently evolve into large-scale, diffuse structures.

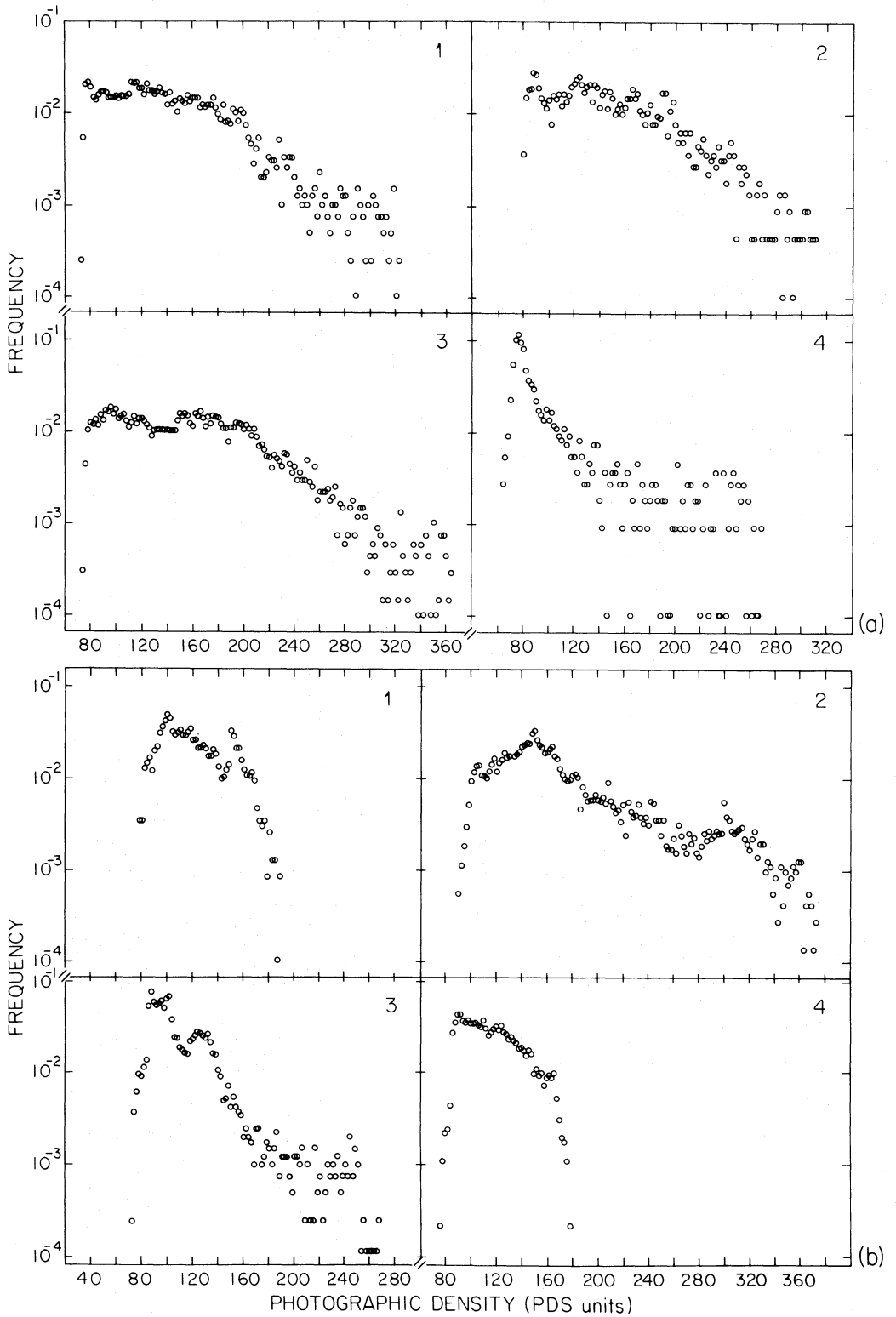

FIG. 4.—Photographic density statistics for two distinct evolving active regions; the monotonic relation between photographic density and energy deposited on film allows one to interpret these statistics in terms of the radiative evolution of the active region. Statistics were obtained on successive solar rotations. Region (*a*) was quiescent for two rotations [182], developed a bright core on the third rotation, and then decayed [4]. Region (*b*) emerged in the first rotation [1], reached its peak brightness on the second rotation [2], and decayed over the next two rotations [3 and 4]. Detailed analysis of these regions, combining the X-ray and EUV data, is in progress (G. Noci, private communication).

particular coronal active region, and shows the decrease in emission (and hence in energy density as well) as the active region ages; this is confirmed by a more quantitative analysis of the evolution of two active regions, shown in Figure 4. The decreasing brightness, and hence decreased average energy density,[1] of evolving active regions is also evident in full-disk X-ray images; see, for example, the synoptic full-disk X-ray images in Vaiana *et al.* (1977).

c) *The range of observed plasma temperatures of quiescent coronal structures is narrow.* By combining data obtained using two different filters, the above quantitative analysis can be refined to yield the line-of-sight average plasma temperature and total emission measure; since the data are in the form of images of the emitting regions, the geometry can be deduced, and it is hence possible to go one step further to obtain line-of-sight plasma electron densities (Vaiana *et al.* 1977). Recently Maxson and Vaiana (1977) have developed a new calibration technique which permits the analysis of regions both in and outside the linear response region of the photographic film. Figure 5 shows one of the results of their work combined with other data, a scatter or correlation diagram of the total photographic density recorded on the film for two filter-wheel positions. The calibration procedure allows one to construct calibration curves corresponding to various line-of-sight average temperatures of the emitting plasma.

[1] We note that although the energy deposited on film is linearly related to the film density (and hence perceived brightness) only in a restricted regime, the actual functional relation is monotonic up to the saturation level of the film; "brighter," therefore, means "greater energy deposition" independent of calibration. Consequently, we can draw the immediate conclusion that the integrated line-of-sight energy density is decreased for larger structures because their brightness is decreased. The increased size, moreover, implies a larger line-of-sight path length L, and therefore the average energy density $\langle N_e T \rangle$ ($\equiv [\int dl N_e T]/L$) is depressed as well, in fact by a substantially larger factor than the integrated energy density.

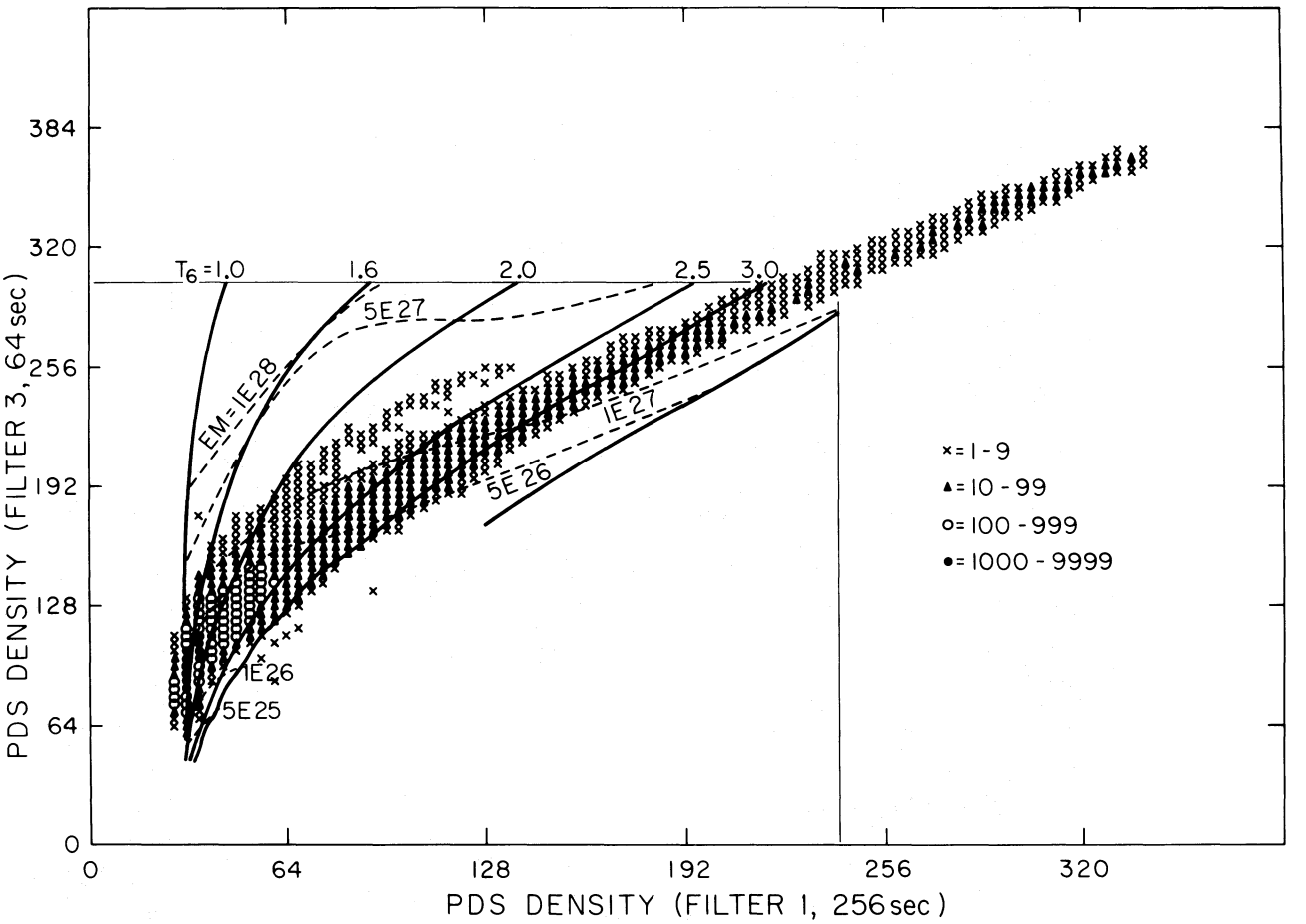

FIG. 5.—Calibrated scatter plot of photographic density of a full-disk image for two filter positions. Note that the number of picture elements associated with given pairs of film densities is indicated. The calibration is due to Maxson and Vaiana (1977), and extends over the low-density and linear regimes of the H-D characteristic film curve; points lying outside the calibrated region are in the saturated density regime for these exposures. Line-of-sight emission measures have been calculated only along the constant-temperature contours; the dashed emission-measure contours were obtained via a spline fit to these calculations. Note that the vast bulk of coronal emission emanates from regions whose temperature lies between 2–3 × 10^6 K.

The most distinctive quantitative result is the relatively narrow observed range for the average coronal plasma temperature of geometrically distinct quiescent coronal features over a huge range of coronal size scales (10^8–10^{10} cm) and plasma densities (10^8–10^{-10} cm^{-3}); see also Davis *et al.* (1975) and Vaiana *et al.* (1976). Spatially averaged EUV emission measure analysis yields similar results (Withbroe 1975). However, it is still possible that small volumes of high-temperature ($T > 3 \times 10^6$ K) material are comingled in the line of sight; the telescope instrument characteristics do not permit us to rule out this possibility. There is nevertheless little doubt that the bulk of coronal material in closed looplike structures—ranging from compact active regions to "quiet Sun" large-scale structures—has a temperature lying within (2–3) $\times 10^6$ K. Particularly striking is the fact that this observed narrow temperature range applies to *distinct* emitting features, which are thermally insulated from one another by the coronal magnetic field (cf. Spitzer 1962); while efficient thermal conduction parallel to the magnetic field for $T > 10^6$ K can be expected to smooth temperature gradients along any one magnetic feature, this cannot be the case of structures with distinct magnetic field topologies. We will in fact show that this behavior can be understood within the context of the model presented in § III below.

d) *Temporal behavior of coronal radiative emission.* Modeling invoking time-independent energy balance is relevant only if observed coronal structures are to some extent stationary. To this end, we note that the observed emission lifetimes of coronal X-ray structures are, generally speaking, far larger than the time scales defined by thermal conduction and radiative emission (cf. Reidy *et al.* 1968; Vaiana and Tucker 1974; Krieger *et al.* 1975); the implication drawn was that continual heating must be present in order to sustain these structures (cf. Gerassimenko, Soladyna, and Nolte 1977 for further details). In fact, a continuous range of time scales exists; these relate both to the overall evolution of the entire active region, measured in terms of the solar rotational period, and to the lifetime of substructures within a given active region, which is of the order of days.

Figures 6*a* and 6*b* exemplify this behavior on two distinct time scales. Although the total (or average) brightness of the complex does not appear to change significantly, the brightness of individual substructures, or loops, can show remarkable variability. Thus, quiescent loop structures can appear relatively unchanged over a time scale of hours (*left column*), but fluctuate over the course of a few days (*right column*). Although the active region as a whole may endure for several solar rotations, its constituent substructures have lifetimes roughly an order of magnitude shorter; in the example shown, the latter lifetimes are significantly larger than the time scales obtained for radiative and uninhibited conductive cooling of nonflaring loop structures (see, for example, Vaiana *et al.* 1976). The presently available data strongly support the applicability of the modeling of §§ III and IV, which presupposes the existence of a relatively stationary state of the loop plasma for quiescent structures on a time scale shorter than their observed fluctuation time scale, e.g., approximately 10^5 s in the case shown here. These models have wider applicability if the observed changes in coronal emission, due to fluctuations in the local coronal heating rate or thermal energy transport along the magnetic field, are simulated by approximating evolving loop structures with a sequence of stationary loop models.

III. THE LOOP MODEL

The steady-state energetics of a coronal loop structure is determined by an energy balance equation of the form

$$E_H + \mathscr{f}\cdot\boldsymbol{v} = \operatorname{div} \boldsymbol{F}_c - E_R + \operatorname{div}\left(\{\tfrac{1}{2}\rho v^2 + U\}\boldsymbol{v} + p\boldsymbol{v}\right), \tag{3.1}$$

where E_H is the local mechanical heating function, $\mathscr{f}$ the net volume force exerted on the fluid by gravity and possibly by the heating mechanism,[2] $\boldsymbol{v}$ the bulk plasma velocity, $\boldsymbol{F}_c$ the thermal conductive flux, E_R the total radiative loss, ρ the plasma mass density, U the plasma thermal energy density, and p the isotropic pressure (see any plasma physics text, such as Rossi and Olbert 1970).

Equation (3.1) is a *local* energy balance relation. By integrating it over the volume of the loop, we obtain the energy balance relation for the loop as a whole:

$$\int_v (E_H + \mathscr{f}\cdot\boldsymbol{v})d^3r = -\int_v E_R d^3r + \mathscr{L}_{\text{footpoints}} + \mathscr{L}_{\text{sides}}, \tag{3.2}$$

where $\mathscr{L}_{\text{footpoints}}$ and $\mathscr{L}_{\text{sides}}$ are the losses (or gains) across the surfaces bounding the cylindrical model loop (Fig. 7). We are implicitly assuming the loops seen in X-ray emission to be spatially coincident with closed coronal magnetic flux tubes; barring the presence of anomalous transport effects, we shall henceforth assume $\mathscr{L}_{\text{sides}}$, which results from cross-field effects, to vanish. This is a good approximation for cross-field heat conduction, but may not be adequate to account for material cross-field drifts (cf. Rosner *et al.* 1977). The advantage of this assumption is, however, that it allows equation (3.1) to be reduced to one-dimensional form.

The other boundary term, $\mathscr{L}_{\text{footpoints}}$, is not as easily accounted for. Energy transport across the footpoint boundaries may be due to either thermal conduction or material transport [e.g., the term $(\frac{1}{2}\rho v^2 + U)\boldsymbol{v}$]. In either

[2] For a wave energy deposition model which neglects wave reflection and refraction, we write $\mathscr{f} = \rho\boldsymbol{g} + \mathscr{f}_w$, where $\boldsymbol{g}$ is the solar gravitational acceleration and $\mathscr{f}_w$ the rate of momentum transfer from the incident wave flux to the fluid. E_H and $\mathscr{f}_w$ are then related via $E_H = \boldsymbol{v}_m\cdot\mathscr{f}_w$, where $\boldsymbol{v}_m$ is the propagation velocity of the heating mode with respect to the fluid.

case $\mathscr{L}_{\text{footpoints}}$ is a boundary condition to be specified in advance, and hence must be determined from semiempirical or theoretical models which are known to accurately account for the boundary layer. In the following, we shall assume $v \to 0$ at the boundaries. This is consistent with a vanishing net mass flux into the loop, a condition derived from the relatively small observed brightness fluctuations of the loops over the time scales of interest (cf. § II above). If one further demonstrates the conductive flux at the base (low chromosphere) to be small, then radiation is the only remaining loss mechanism for a closed, quiescent loop; conduction then serves only as an energy redistribution mechanism.

The present aim is to demonstrate that many of the essential elements of coronal loop physics can be discussed within a conceptually simple framework, one in which the principal results are analytically rather than numerically derived. In order to do so, we require two additional assumptions: (1) $v \sim 0$, (2) p is constant along the field. Our calculations will show the first assumption to be consistent with the X-ray observations of quiescent coronal structures. The second assumption is reasonable as long as the height of the loop above the solar surface is small when compared with the pressure scale height H,

$$h_{\text{loop}} \ll H = 5 \times 10^3 T \text{ cm}, \tag{3.3}$$

where T is the temperature; since our discussion focuses upon active-region loops, this useful simplification is a rather good approximation.[3]

The temperature and density distribution in the loop is then determined by the simpler energy balance relation

$$E_H + E_R - \text{div } F_c = 0 \tag{3.4}$$

and the boundary conditions, which we shall assume to be

$$T(s = 0) = T_0 = 2 \times 10^4 \text{ K}, \tag{3.5}$$

$$F_c(s = s_{\max}) = 0, \tag{3.6}$$

where F_c is the conductive heat flux parallel to the magnetic field,

$$F_c(s) = -\kappa T^{5/2} \frac{dT}{ds} \sim -10^{-6} T^{5/2} \frac{dT}{ds}, \tag{3.7}$$

and $s_{\max}$ the coordinate of the top of the loop as measured along the magnetic field; without loss of generality, we have assumed the loop to be symmetric about $s = s_{\max}$. The radiative loss function can be written as

$$E_R = -(p^2/4k^2T^2)P(T) \text{ ergs cm}^{-3} \text{ s}^{-1}, \tag{3.8}$$

where $P(T)$ is a function which may be analytically approximated by a sequence of power laws joined continuously, each having the form (see Appendix A)

$$P(T) = \alpha_{ij} T^{\beta_{ij}}, \qquad T_i < T < T_j. \tag{3.9}$$

The functional form of these relations suggests that equation (3.4) be written with T as the independent variable (Landini and Fossi 1975); we obtain

$$-\text{div } F_c = \frac{d}{ds}(\kappa T^{5/2} dT/ds) = (F_c/\kappa T^{5/2})(dF_c/dT), \tag{3.10}$$

and, with the aid of equations (3.8) and (3.10), equation (3.4) reads instead

$$(F_c/\kappa T^{5/2})(dF_c/dT) = (p^2/4k^2T^2)P(T) - E_H. \tag{3.11}$$

Equation (3.11) can be integrated to obtain the thermal conductive flux as a function of temperature:

$$F_c^2(T) - F_c^2(T_0) = (\kappa p^2/2k^2)\int_{T_0}^{T} dT' T'^{1/2} P(T') - 2\kappa \int_{T_0}^{T} dT' T'^{5/2} E_H(T'). \tag{3.12}$$

[3] We note that although this argument applies only to the coronal, X-ray emitting portion of a loop, $p \sim$ constant obtains at lower temperatures as well because of the large temperature gradient in the transition zone. That is, the transition region temperature scale height is small when compared with the pressure scale height at corresponding temperatures; thus $p \sim$ constant applies near the relatively cool loop footpoints as well (cf. Athay 1976, p. 278).

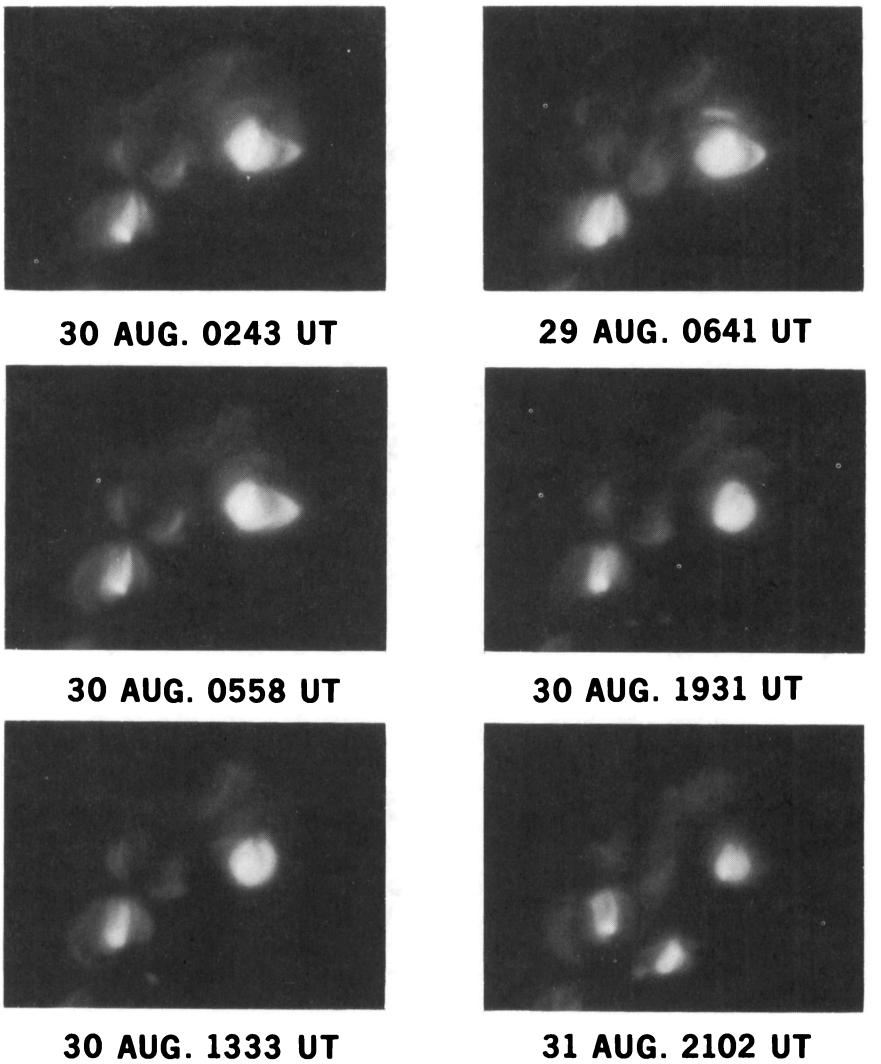

FIG. 6.—Moderate time resolution quiescent active region evolution. On a time scale of hours (*left column*), only individual loop structures show some variation, while substantial rearrangements of loop complexes appear to require a few days (*right column*).

In order to simplify the appearance of the equation, we define the auxiliary functions

$$f_R(T) \equiv (\kappa p^2/2k^2)\int_{T_0}^{T} dT' T'^{1/2} P(T') , \tag{3.13}$$

$$f_H(T) \equiv 2\kappa \int_{T_0}^{T} dT' T'^{5/2} E_H(T') , \tag{3.14}$$

where f_R and f_H represent the radiation loss and energy deposition contributions to the thermal conductive flux; $f_R(T)$ can be approximated by (see Appendix A):

$$f_R(T) \sim (\kappa p^2/2k^2)\cdot \begin{cases} 10^{-29.0} T^3, & T < 10^{5.1} \\ 10^{-18.8} T, & T > 10^{5.1} \end{cases} \tag{3.13'}$$

In general we expect $F_c^2(T_0) < 10^4$, whereas $f_R(T)$ and $f_H(T) > 10^{10}$; the coronal temperature and density structure is, therefore, quite insensitive to the base conductive flux, and hence $F_c^2(T_0)$ will be neglected in the following (cf. McWhirter, Thonemann, and Wilson 1975 and Athay 1976, p. 278). Equation (3.12) then becomes

$$F_c^2(T) \sim f_R(T) - f_H(T) . \tag{3.15}$$

Finally, we obtain the variation of temperature with distance along the flux tube by using equations (3.7) and (3.15):

$$s(T) - s(T_0) = \int_{T_0}^{T} dT' T'^{5/2} [f_R(T') - f_H(T')]^{-1/2} . \tag{3.16}$$

Both $f_R(T)$ and $f_H(T)$ are monotonically increasing functions of T, as can be seen from equations (3.13) and (3.14). Inspection of equation (3.15) shows further that for any physically meaningful solution, $f_R > f_H$ everywhere. Equality is obtained when the total energy deposition within the loop balances the total radiative losses, so that the conductive flux vanishes and the temperature maximum is obtained; this condition also maximizes $s(T) - s(T_0)$. The conductive flux thus approximately vanishes at $s(T_0)$ and exactly vanishes at $s(T_{\max})$. The extremum of F_c (in fact, the maximum) occurs when the local radiative loss equals the local energy deposition rate:

$$(p^2/4k^2 T_1^2) P(T_1) = E_H(T_1) \tag{3.17}$$

(cf. eq. [3.11]), where $T = T_1$ is the temperature at which equality obtains. Thus, for $T_0 < T < T_1$, we have $E_R > E_H$, while for $T_1 < T < T_{\max}$, $E_R < E_H$.

In the following, we use the above formalism, in conjunction with observed restrictions upon the geometries of the loops, to test various simple models for nonradiative energy deposition in the corona.

IV. MODEL RESULTS

a) Loop Geometry and Thermal Stability

Up to this point, the length of the loops, and hence their geometry, have not entered into our analysis; therefore, the temperature profiles as a function of height obtained from equation (3.16) will in general yield an essentially arbitrary position of the temperature maximum, $s = s(T_{\max})$. That is, a coincidence of $s(T_{\max})$ with the position of the apex of the loop ($s = s_{\max}$; cf. Fig. 7*a*) for arbitrary values of the base pressure must be accidental in the absence of additional constraints. Rather simple physical considerations show, however, that when the geometry of hydrostatic loops is considered, the only physical solutions are those for which $s(T_{\max}) = s_{\max}$.

Consider first the case $s(T_{\max}) < s_{\max}$, so that the temperature maximum lies below the top of the loop; the total radiative losses balance the total mechanical energy deposited in the interval $s(T_0) < s < s(T_{\max})$ (Fig. 7*b*). Since the temperature maximum coincides with the position of zero conductive flux, the plasma lying between $s(T_{\max})$ and the loop apex ($s = s_{\max}$) can rid itself of the deposited mechanical energy only via radiation; thermal conduction to plasma lying below $s(T_{\max})$ is excluded by definition, and therefore the portion of the loop lying between $s(T_{\max})$ and the top is energetically isolated from the remainder. Thus the total mechanical energy deposited above $s = s(T_{\max})$ must balance exactly the total radiative losses above the temperature maximum to maintain equilibrium. This condition is thermally unstable.

Fluctuations in the heating rate leading to an increase in the average temperature for $s > s(T_{\max})$ will decrease the total radiative loss rate E_R in this region because $\partial E_R/\partial T < 0$ for temperatures greater than 3×10^5 K for constant-density perturbations, and greater than 10^5 K for isobaric perturbations (cf. Appendix A). This runaway process is not stabilized by thermal conduction until the temperature within $s(T_{\max}) < s < s_{\max}$ has exceeded $T_{\max}$; the temperature maximum will thus move to the top of the loop. Similarly, we can show that fluctuations yielding a decrease in the average temperature within $s(T_{\max}) < s < s_{\max}$ are unstable as well; here the position of

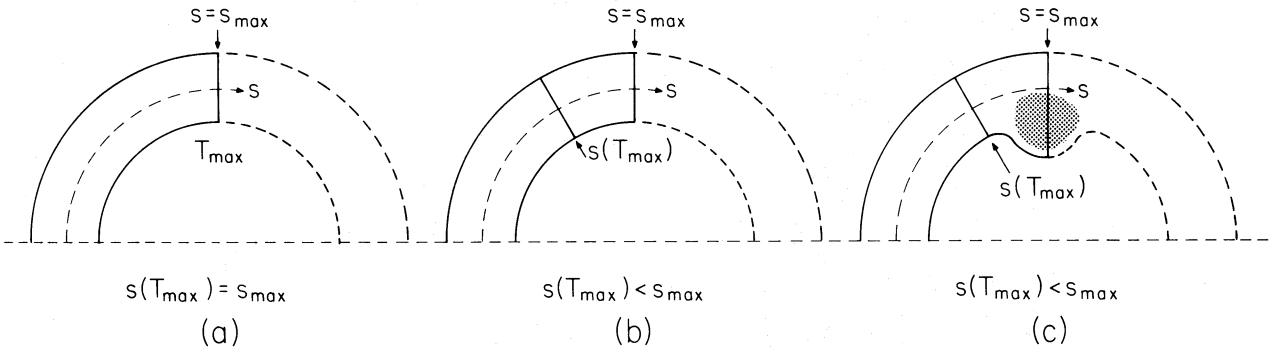

FIG. 7.—Possible loop configurations. (*a*) The equilibrium configuration whose temperature maximum is located at the top of the loop, corresponding to quiescent coronal X-ray loops. (*b*) A thermally unstable loop configuration. (*c*) A loop geometry which allows the temperature maximum to lie below the top of the loop and yet maintain equilibrium; this configuration may correspond to the formation of stable condensations of plasma in the corona.

the temperature maximum is forced downward, and the entire loop cools and collapses back down to the lower chromosphere.[4]

For the case $s(T_{max}) > s_{max}$, the temperature is still increasing at the top of the loop; that is, $dT/ds \neq 0$ at $s = s_{max}$. The physical meaning of this condition is that insufficient mechanical energy deposition has occurred to balance the total loop losses. Therefore, the entire loop will cool; this again aggravates the problem since radiative cooling increases with decreasing temperature (see above). The matter in the loop cools, and again falls back down to the chromosphere.

These arguments apply to loops seen in X-rays, for which the average coronal temperature exceeds 10^6 K. *Coronal* loops at sufficiently low average temperature that the above arguments fail ($T_{average} < 3 \times 10^5$ K) will nevertheless not be in hydrostatic equilibrium for geometric configurations shown in Figures 7*a* and 7*b* because the pressure scale height corresponding to these low average temperatures is too small to account for the hydrostatic support of the cool plasma (Foukal 1976).

However, static equilibrium can be maintained for $s(T_{max}) < s_{max}$ at low average coronal temperatures if the cooler plasma lying above the temperature maximum is supported by forces other than the gas pressure; one possibility is shown in Figure 7*c*, which may correspond to the formation of quiescent prominences supported by magnetic fields within loop structures. We conjecture that such configurations may arise when the condensation process resulting from the above instability is sufficiently rapid that the local magnetic field deforms to provide a local gravitational potential well (Fig. 7*c*) before the matter can flow down along the loop toward the chromosphere.[5]

We thus conclude that hydrostatic quasi-stationary loop structures must correspond to solutions of equation (3.16) with the additional constraint

$$s(T_{max}) = s_{max}, \tag{4.1}$$

so that the temperature maximum is located at the top of the loop; these loop structures we identify with the quiescent loops seen in the X-ray corona. Furthermore, we find that departures from this equilibrium state (e.g., eq. [4.1]) lead to loop plasma configurations which may account for much of the dynamics of the nonflaring corona. Thus, transient loop brightenings seen in X-rays (Fig. 6 and Vaiana *et al.* 1973) can be explained by noting that heating fluctuations above the quiescent level—with the loop size fixed—lead to an increased loop pressure if equilibrium is to be maintained (cf. eq. [4.4] below); consequently, the loop emission measure rises, and the loop appears brighter.

Cool coronal structures in this picture are the result of local loop heating which is insufficient—in a time-averaged sense—to maintain the loop atmosphere in a dynamically stable state at high coronal temperatures; we conjecture that these loops are dominated by heating fluctuations which yield successive cycles of plasma rapidly filling loops (the relevant time scale here determined by the rate of onset of heating) and consequently cooling and collapsing back down to the footpoints. This suggestion may explain the presence of cool coronal loops seen in EUV emission lines (Foukal 1976) and the recently reported persistent downflows observed at levels corresponding to loop footpoints (cf. Bruner *et al.* 1976). Furthermore, as noted above, such heating supply fluctuations may lead to prominence formation if the time scale for condensation falls below that defined by the downflow.

[4] These instabilities are related to those discussed, for example, by Field (1965), with the crucial additional constraint of a perfectly insulating boundary [e.g., conductive flux vanishes at $s = s(T_{max})$].

[5] This geometric configuration, but not the formation mechanism, is similar to that proposed by Pikeln'er (1971).

b) Energy Deposition Scale Length and Loop Stability

The previous argument can be extended to the spatial dependence of the coronal heating function. We restrict our discussion to inferences which can be drawn directly from the present model; further comparisons with specific heating models (as discussed in Appendix B) are drawn in § IV*d* below.

Consider the extreme case pictured in Figure 8*a*: all heating occurs in a thin layer located at $s = s_1$, close to the base of the loop; thermal conduction therefore must provide the means by which energy is redistributed within the loop interior. Outside the heated region the energy equation has the simple form

$$\text{div } F_c = E_R = \frac{p^2}{4k^2T^2} P(T) . \tag{4.2}$$

Consider the solution $T = T(s)$ for $s > s_1$; from equation (4.2) we obtain $dT/ds < 0$, and hence $T(s) < T(s_1)$ for $s > s_1$. This contradicts our previous conclusion that the temperature maximum is located at the top of the loop, a result based upon thermal stability considerations. The proposed heating function can be excluded on the basis of a mechanical stability analysis as well. As p is assumed to be constant, the density $n = n(s)$ must be an increasing function of height for $s > s_1$. This configuration is well known to be subject to the Rayleigh-Taylor instability (Landau and Lifshitz 1959), and hence cannot be stable. A less extreme heating function as shown in Figure 8*b* can be dealt with in precisely the same manner.

The above *mechanical* stability argument is somewhat relaxed if one allows the pressure to vary within the loop [e.g., $p = p(s)$]. In hydrostatic equilibrium both the pressure scale height λ_p [$\equiv p/(dp/ds)$] and the density scale height λ_n [$\equiv n/(dn/ds)$] must be negative; the latter requirement ensures suppression of the Rayleigh-Taylor instability. As $\lambda_n = \lambda_p\lambda_T/(\lambda_T - \lambda_p)$ with λ_T [$\equiv T/(dT/ds)$] the temperature scale height, stability imposes the condition that either $\lambda_T > 0$ (obtained if $T_{\max}$ is located at the top of the loop), or that $|\lambda_T| > |\lambda_p|$ in the case at hand. The latter condition is satisfied if the upward conductive flux does not exceed $\sim 2 \times 10^5 T_6^{5/2}$ ergs s^{-1} cm^{-2}; this modest requirement can be satisfied under typical coronal conditions ($T_6 \sim$ 2–3). However, the *radiative* stability argument remains in force, as it does not depend upon the assumption of constant pressure; the heating functions depicted in Figures 8*a* and 8*b* are therefore still excluded, even for loops comparable in size with the pressure scale height.

The remaining possibilities which are allowed are shown in Figures 8*c* and 8*d*. We caution that these sketches are meant only to suggest the general—not the detailed—spatial dependence of the heating function; thus, an exponentially varying heating function $E_h \sim E_0 \exp(-s/s_M)$ will be acceptable if the damping scale length s_M is not small when compared with the loop length ($s_{\max} - s_0$). The crucial point is that significant heating must extend to the top of the loop and therefore that coronal heating models with short (in the sense above) deposition scale heights can be excluded; observational evidence supporting this conclusion has been discussed previously by Neupert, Nakagawa, and Rust (1975).

c) The Maximum Loop Temperature as a Function of the Loop Pressure and Loop Size

The simplest model one can construct using the formalism developed in § III is based upon the assumption that the heating function is a constant (in space), independent of the local values of p and T. Using equations (3.8), (3.13′), (3.16), and (4.1) together, we can eliminate E_H to obtain

$$T_{\max}(s = s_{\max}) \approx 1.4 \times 10^3 (pL)^{1/3} . \tag{4.3}$$

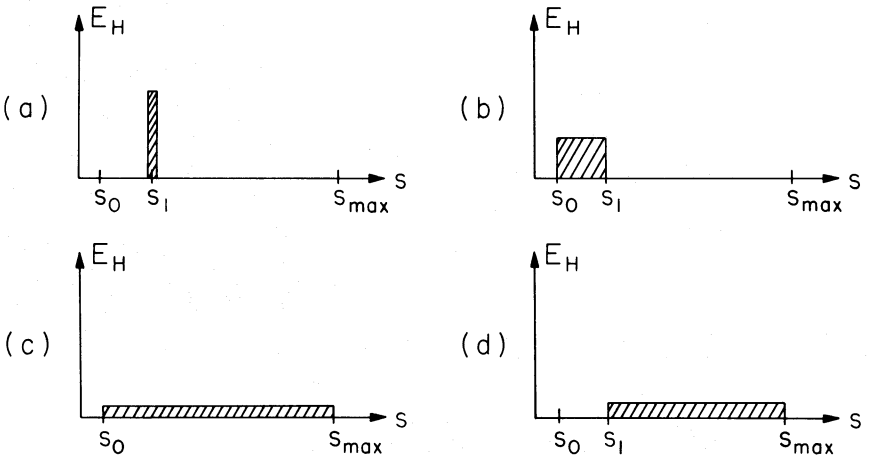

FIG. 8.—Four idealized functional forms for the spatial dependence of the coronal loop heating function. (*a*) Energy deposition in a thin layer Δs at $s = s_1, s_0 < s_1 < s_{\max}$ with $\Delta s_{\max} \ll s_{\max} - s_0$. (*b*) Deposition only near the loop footpoint. (*c*) Uniform deposition along the entire length of the loop. (*d*) Uniform deposition, starting above $s = s_1$, $s_0 < s_1 < s_{\max}$.

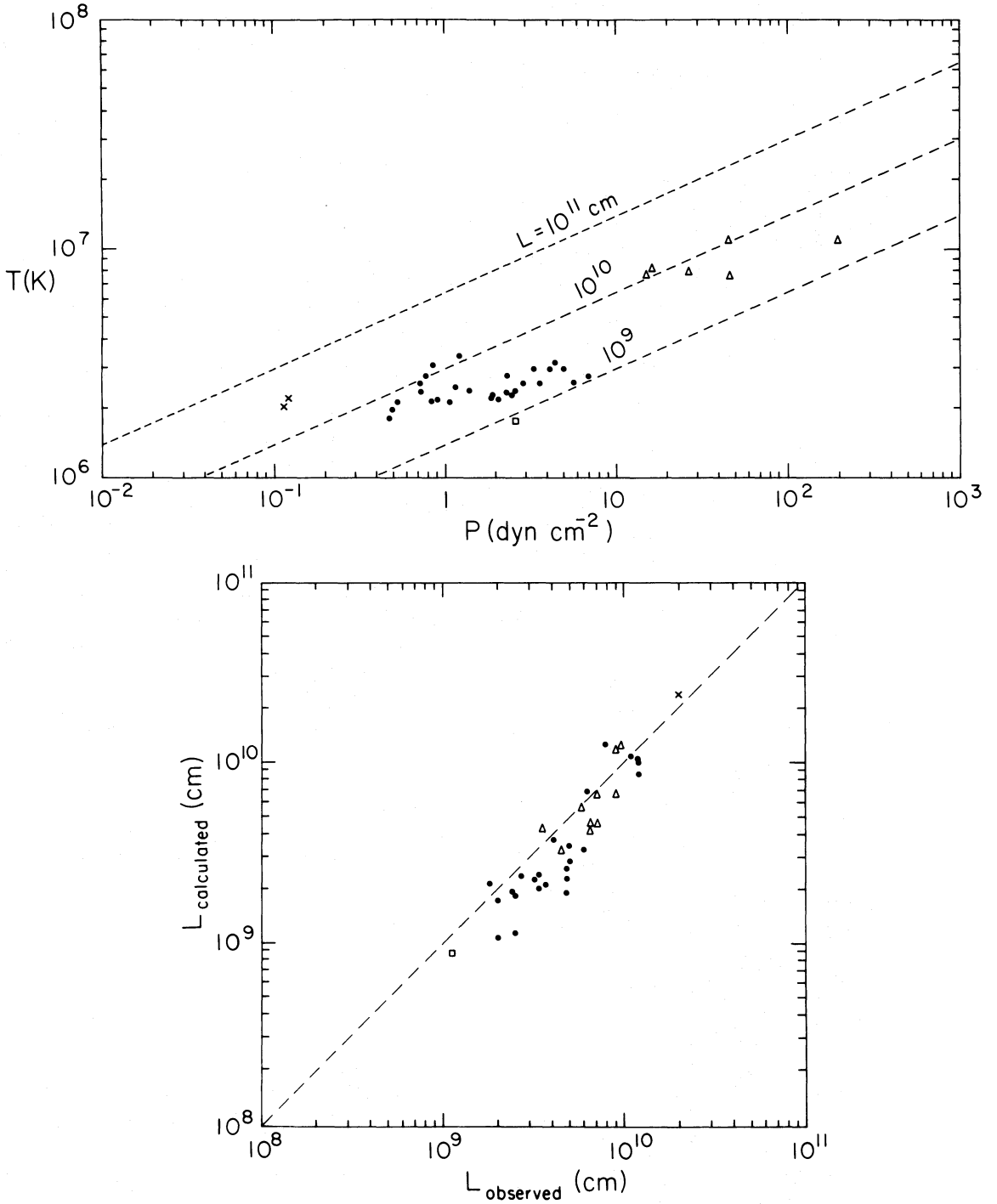

FIG. 9.—(*a*) Plasma temperature and pressure for a variety of coronal structures, ranging from large-scale loop structures (*crosses*: Maxson and Vaiana 1977) to bright points (*open square*: L. Golub, private communication), active region loops (*filled circles:* Landini *et al.* 1975; Pye *et al.* 1977; R. Chase, private communication), and large, prominence-related flare loops (*open triangles:* Pallavicini *et al.* 1977). Also indicated is the theoretically predicted variation of the plasma temperature with loop pressure, with loop size L as a parameter (eq. [4.3]). (*b*) Comparison of predicted loop size (via eq. [4.3] and the temperatures and pressures from Fig. 9*a*) with observed loop size. Note that virtually all points fall within a factor of 2 of their predicted loop size. Not shown are the results for compact flaring structures; for these, $L_{\rm calculated} \gg L_{\rm observed}$. This is to be expected, since such structures have unusually large emission measures for their size.

where L is the loop length ($s_{\max} - s_0$). We have plotted $T_{\max}(p)$, with L as a parameter, in Figure 9*a*, as well as typical values of (p, T) for a variety of coronal X-ray structures, ranging from flaring loops (Pallavicini, Serio, and Vaiana 1977) to large-scale structure loops (Maxson and Vaiana 1977). The observations are directly compared with theory in Figure 9*b*, in which we plot the observed loop length versus the calculated loop length obtained by using the values of (p, T) shown in Figure 9*a* in equation (4.3). The observed sizes all fall within a factor of 2 of the predicted scale lengths. We note that our model contains no free parameters, and hence is not adjusted to fit the data. The significance of our result is therefore that, to the accuracy quoted above, both the absolute values and the trend of loop sizes can be predicted on the basis of a hydrostatic, closed-loop atmosphere without the necessity of model parameter fitting. The next step, for a more sophisticated modeling ot the corona, will require additional constraints, as for example provided by EUV data used in conjunction with X-ray observations; see Appendix C.

In the case of the extremes of coronal structuring (e.g., flare loops and large-scale structures), the agreement is somewhat surprising, since the assumptions upon which the model is based (e.g., p = constant, $v = 0$) are generally thought to be invalid in these cases. Indeed, compact flare loops are not accounted for by our model; only the large loop flares associated with prominence activation appear to be sufficiently close to hydrostatic equilibrium. Furthermore, in the case of large-scale structure loops, the observed loop length is that of the largest, unambiguously closed loop structures; these are still sufficiently compact to expect our model to be applicable. Larger loop structures, such as those for which only footpoints can be observed in X-ray images, or ones associated with helmet structures seen in white light coronagrams, are not fitted by this model.

Nevertheless, coronal loop structures appear to obey a simple rule over virtually their entire range: that the structure size determines the locus of allowed temperatures and pressures, while the heating function fixes the loop's position along that locus. Furthermore, the correlation between the observed and calculated loop lengths (Fig. 9*b*) is consistent with our initial hypothesis that coronal loops seen in X-rays are not far from hydrostatic equilibrium.

d) Dependence of Heating Function upon Loop Parameters

For the moment we consider the simple heating model just discussed. By using equations (3.15), (4.3), and the fact that the conductive flux vanishes at the temperature maximum, we can eliminate $T_{\max}$ in order to obtain E_H as a function of the parameters defining the loop; thus

$$E_H \approx 9.8 \times 10^4 p^{7/6} L^{-5/6} . \tag{4.4}$$

In very general terms the dependence is as expected: the pressure, which controls the radiative loss rate, is positively correlated with the heating rate; furthermore, this simple model shows the desired trend of decreased energy deposition with increased loop size (see discussions in § II). On a somewhat more detailed level, we may compare equation (4.4) with the results of Appendix B, in which we have calculated the expected parametric dependence of the heating functions for a variety of heating models.

We first note that coronal heating theories which predict a dependence of E_H upon the local temperature cannot be directly considered because our loop models assume E_H to be spatially uniform. Thus only Alfvén mode dissipation and current heating, as formulated in Appendix B, can be directly tested against the predictions of equation (4.4). In both of these cases the agreement between equation (4.4) and the expressions derived in Appendix B is good, with Alfvén wave damping at some advantage because the heating function's inverse dependence upon loop size is built into the model at the onset.

However, the arguments adduced in § IV*b* above concerning the spatial dependence of the energy deposition remain in force and can be applied to the remaining heating functions. In particular, we have argued that heating functions whose deposition scale height was small when compared with the loop scale size are not consistent with high coronal temperatures at the top of loops. In this connection we note that both acoustic mode shock heating and anomalously damped Alfvén mode heating have a strong inverse temperature dependence (cf. Appendix B), which leads to a rapid decrease of the rate of local energy deposition with height in the transition zone. These heating modes therefore cannot be reconciled with the observed coronal loop structures.

Viscous damping of acoustic modes has as yet not been considered. As a direct heating mechanism, this model can be ruled out both because acoustic modes are thought to shock before entering the corona (cf. Stein and Leibacher 1974) and because the associated damping scale length is much smaller than typical loop sizes (see below). However, the Alfvén dissipation mechanism discussed by Wentzel (1974), which appears to meet the criteria set by our simple model, involves the conversion within loops of Alfvén modes to acoustic modes; the latter modes must damp rapidly in order for the heat to be deposited *within* the loops. Thus viscous acoustic mode damping is viable if it is viewed as a secondary heating effect, and if the dissipation length is sufficiently small. From equation (B.2a) we find that

$$\lambda(\text{viscous damping}) \approx 1.2 \times 10^8 \text{ cm} \tag{4.5}$$

for $p \approx 0.1$ dyn cm^{-2} and $T \approx 2.5 \times 10^6$ K; this distance is small when compared with typical active region loop dimensions and therefore argues for this mechanism.[6]

V. SUMMARY AND DISCUSSION

We have developed an analytic model for coronae based upon the hypothesis that looplike structures are the basic coronal building block, a point of view strongly supported by the available data for the solar corona. Starting with the assumption that quiescent loop structures seen in X-rays are in hydrostatic equilibrium, we demonstrate that such loops must have their temperature maximum located near their apex, and that significant nonradiative energy deposition must occur along most of their length. The calculations yield a unique relation between the loop temperature, pressure, and size (eq. [4.3]) which fits the X-ray observations of quiescent structures well, and is consistent with the initial assumption of hydrostatic equilibrium for such structures.

Our results therefore suggest that the coronal loops visible in X-rays represent a relatively stationary equilibrium of the confined plasma, and that fluctuations in, for example, the local heating rate can lead to dynamically unstable states in which the loop plasma does not attain temperatures sufficient for significant X-ray emission. These unstable states may correspond to the relatively cool coronal loops seen in EUV emission lines (Foukal 1976); the decay of unstable hot, X-ray emitting loops to a cool, EUV emitting state then may explain the presence of reported downflows at atmospheric levels corresponding to loop footpoints (cf. Bruner *et al.* 1976). From this perspective, the formation of quiescent prominences within loop structures obtains if the time scale for local condensation dominates that defined by the downflow of plasma (§ IV*b*). Correspondingly, transient X-ray loop brightenings may result from the response of the equilibrium loop atmosphere to a transient excess of coronal heating. Furthermore, a parametrization of various proposed coronal heating theories is developed within the context of the model; it shows that only magnetic-field–related heating theories, such as Alfvén-mode dissipation and localized coronal current heating, are consistent with the observations.

The ability of as simple a theory as developed here to account for the gross features of the inhomogeneous solar corona calls into question theories of stellar coronae based upon homogeneous (plane-parallel or spherically symmetric) modeling. The solar X-ray corona exhibits structures associated with a wide dynamic range of plasma densities and length scales. If one makes the reasonable presumption that stellar coronae other than the Sun's are similarly structured, then spatially unresolved observations of such coronae represent a statistical smoothing of widely disparate plasma structures, and direct modeling of such averaged data is not likely to be representative of the actual physical conditions.

As an alternative, we suggest that models for discrete coronal structures, such as presented here, can be used to generate a statistical description of a stellar corona. Our model relates the size of a coronal structure to its temperature and density; it may therefore be possible to construct a model corona which consists of a variety of various-sized structures, the precise mix to be determined by the radiative properties of the corona viewed in its entirety. The Sun can be used as a calibration standard because spatially resolved observations are available both to test the model chosen for individual loop structures, and to assemble the proper choice of variously sized loop structures with the total radiative properties characteristic of the solar corona. The later modeling can be done during the course of the solar cycle, thus providing a measure for the appropriate statistical mix of structures over the entire dynamic range of solar coronal emission. The results of such a theory, when applied to other stars, may assist in revealing the physical condition in stellar coronae other than the Sun's; the present effort represents a first step in this direction.

We wish to extend our thanks to C. Maxson for substantial help with the data analysis; to R. Chase for providing unpublished data; to J. Raymond for advice regarding coronal radiative losses; to P. Foukal for comments regarding coronal structure, particularly as seen in the EUV; and to L. Golub and an anonymous referee for aid in clarifying our discussions.

This work was supported by NASA contract NAS8-31374 at the Harvard College Observatory and by the Langley-Abbot Program of the Smithsonian Institution.

APPENDIX A

CORONAL RADIATIVE LOSSES

The time-independent radiative loss function[7] $P(T)$ for an optically thin plasma has been calculated by a number of independent workers (Pottasch 1965; Cox and Tucker 1969; Tucker and Koren 1971; McWhirter *et al.* 1975; Raymond 1978). Comparison of these calculations shows that there are a number of significant discrepancies, particularly at chromospheric ($\sim 2 \times 10^4$ K) and transition zone temperatures (see Fig. 10). The differences arise

[6] We must caution, however, that this size scale is not small when compared with compact coronal features such as bright points. The heating of compact coronal structures by Alfvén modes is, therefore, open to some doubt.

[7] The quantity $n_e n(H) P(T)$ is the power radiated per unit volume.

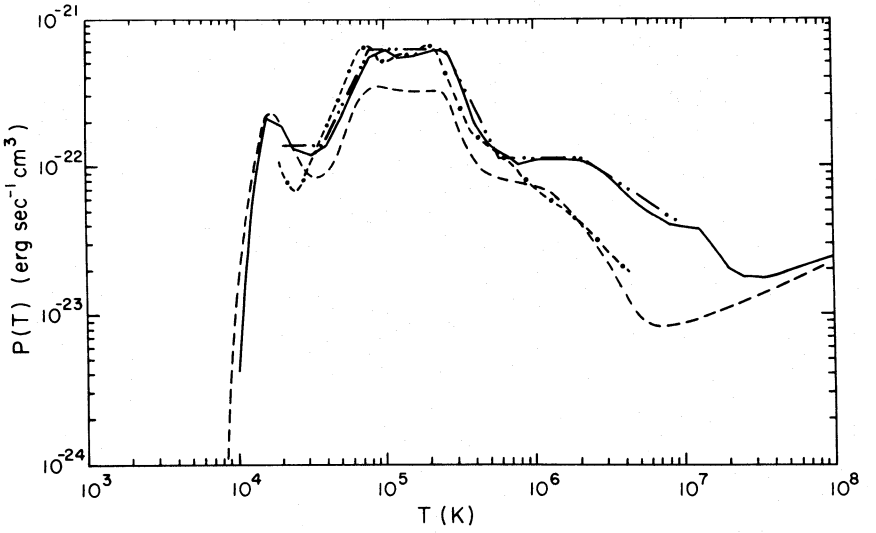

FIG. 10.—Comparison of various radiative loss functions. Shown are the results of Pottasch (1965) [·—·—·], McWhirter *et al.* (1975) [———], Raymond (1978) [——], and our analytic fit to Raymond's curve [· ·—· ·, eq. (A.1)].

from three independent concerns: (1) the nature (accuracy) of the atomic physics calculations; (2) the accuracy of the atomic physics parameters (e.g., cross sections); (3) the values of the relative elemental abundances used in the calculations. Whereas there have been substantial advances in the first two areas, the problem of accurately determining relative abundances in the solar corona is still controversial; we refer the reader to Davis *et al.* (1975) and the recent review by Withbroe (1976) for details.

As a consequence of the uncertainties attendant upon the detailed calculation of $P(T)$, it is reasonable to approximate the radiative loss function by an analytic expression as long as (*a*) the approximation lies within the estimated error bounds of the best detailed calculations, and (*b*) no crucial results depend upon the detailed functional form of the approximation. The latter injunction is particularly important because the goodness of fit on a log-log plot, as in Figure 10, is quite deceptive; thus, quantities such as $dP(T)/dT$, which are of importance in thermal instability analysis, are very sensitive to the detailed fit. With these cautions in mind we have generated an analytical fit to $P(T)$, using a detailed calculation provided by Raymond (1978) for solar abundances; the approximation is shown in Figure 10 and is given by the expression

$$\begin{aligned}
P(T) &\approx 10^{-21.85} && (10^{4.3} < T < 10^{4.6}\ \mathrm{K}) \\
&\approx 10^{-31}T^{2} && (10^{4.6} < T < 10^{4.9}\ \mathrm{K}) \\
&\approx 10^{-21.2} && (10^{4.9} < T < 10^{5.4}\ \mathrm{K}) \\
&\approx 10^{-10.4}T^{-2} && (10^{5.4} < T < 10^{5.75}\ \mathrm{K}) \\
&\approx 10^{-21.94} && (10^{5.75} < T < 10^{6.3}\ \mathrm{K}) \\
&\approx 10^{-17.73}T^{-2/3} && (10^{6.3} < T < 10^{7}\ \mathrm{K}).
\end{aligned} \tag{A1}$$

In addition we require the auxiliary function $f_R(T)$ (cf. eqs. [3.12] and [3.13]); using equation (A1), we obtain

$$\begin{aligned}
\int_{T_0}^{T} dT'T'^{1/2}P(T') &\approx 10^{-21.97}T^{1.5} - 10^{-15.52} && (10^{4.3} < T < 10^{4.6}\ \mathrm{K}) \\
&\approx 10^{-31.54}T^{3.5} - 10^{-15.74} && (10^{4.6} < T < 10^{4.9}\ \mathrm{K}) \\
&\approx 10^{-21.38}T^{1.5} - 10^{-14.28} && (10^{4.9} < T < 10^{5.4}\ \mathrm{K}) \\
&\approx 10^{-12.68} - 10^{-10.1}T^{-0.5} && (10^{5.4} < T < 10^{5.75}\ \mathrm{K}) \\
&\approx 10^{-22.12}T^{1.5} + 10^{-13.17} && (10^{5.75} < T < 10^{6.3}\ \mathrm{K}) \\
&\approx 10^{-17.65}T^{5/6} - 10^{-12.94} && (10^{6.3} < T < 10^{7}\ \mathrm{K})
\end{aligned} \tag{A2}$$

where

$$f_R(T) = \frac{\kappa p^2}{2k^2}\int_{T_0}^{T} dT' T'^{1/2} P(T') .$$

The latter integral is well fitted over the interval 2×10^4 K $< T < 10^7$ K by

$$\int_{T_0}^{T} dT' T'^{1/2} P(T') \approx 10^{-29.04} T^3 \quad (T < 10^{5.11})$$

$$\approx 10^{-18.81} T \quad (T > 10^{5.11}) . \tag{A3}$$

APPENDIX B

CORONAL HEATING MODELS

We consider three different models for the deposition of mechanical energy in the corona; these are heating via (1) dissipation of acoustic modes; (2) Alfvén wave damping; (3) direct dissipation of coronal currents. These three models are distinguished by the consequent functional dependence of the heating rate E_H upon the loop pressure p, the loop temperature T, and possibly the loop geometry; our discussion is meant only to elicit these general parametric functional relations, and is therefore not intended as a study of the detailed physics of the deposition mechanisms. Previous, more detailed treatments can be found in Stein and Leibacher (1974) and Wentzel (1974), and related discussions by Jordan (1976) and McWhirter and Wilson (1976).

a) Wave Dissipation

The rate of energy deposition by a wave mode depends upon the magnitude of the energy flux $\boldsymbol{F}$ and the damping scale length λ; thus E_H is given by

$$E_H = -\operatorname{div} \boldsymbol{F} \approx \lambda^{-1} F \text{ ergs s}^{-1} \text{ cm}^{-3} . \tag{B1}$$

The relevant damping scale length depends critically upon the dominant dissipation mechanism; thus we have

A. Acoustic modes[8]:

1. Viscous damping (Lamb 1909; Zel'dovich and Raizer 1968):

$$\lambda \approx 7.53 \times 10^{21} p T^{-2} \text{ cm} . \tag{B2a}$$

2. Shock-wave dissipation:

$$\lambda \approx 1.43 \times 10^{6} T^{1/2} \text{ cm} . \tag{B2b}$$

B. Alfvén modes:

1. Conduction damping (Jackson 1962; Braginskii 1965):

$$\lambda \text{ (classical resistivity)} \approx 1.16 \times 10^{-4} p^{3/2} T^3 B^3 \tau^2 \frac{20}{\ln \Lambda} \text{ cm} . \tag{B3a}$$

For demonstrative purposes only we calculate the dissipation length for Alfvén modes entering a region subject to strong Langmuir turbulence:

$$\lambda \text{ (anomalous resistivity)} \approx 3.23 \times 10^{3} p^{-1} T B^3 \tau^2 \text{ cm} . \tag{B3b}$$

2. Viscous damping (Braginskii 1965):

$$\lambda \approx 2.1 \times 10^{-6} p^{-5/2} T^3 B^5 \tau \frac{20}{\ln \Lambda} \text{ cm} . \tag{B3c}$$

In the weak-field limit (e.g., $\omega_{gi}\tau_{ci} < 1$, ω_{gi} the ion gyrofrequency and τ_{ci} the ion self-collision time), this result is modified to read

$$\lambda \approx 3.3 \times 10^{15} p^{-1/2} T^{-2} B^3 \tau^2 \frac{20}{\ln \Lambda} \text{ cm} . \tag{B3d}$$

[8] We have set the wave period $\tau = 300$ s.

3. Mode conversion via field curvature (Wentzel 1974):

$$\lambda \approx R \text{ cm}, \tag{B3e}$$

where R is the loop radius of curvature.

Direct computation immediately shows that the Alfvén mode damping lengths for classical conduction and viscous damping are much larger than typical scale lengths of inner coronal structures, and therefore these processes can be eliminated from further consideration.

In the present simplified parametrization we assume that the incident flux F is proportional to the base pressure, and hence that the total energy input at the base of the loops is the same for all models; this can be justified by arguing that the total thermal energy content of a loop (which is proportional to the base pressure) is itself proportional to the total energy input at the base. In order to eliminate the magnetic field from the above equations, we introduce the further assumptions that

$$B^2 \propto p; \qquad B \propto R^{-3}, \tag{B4}$$

where R is a loop scale length (possibly the loop radius of curvature). Using equation (B1) together with the dissipation lengths quoted above, we find the functional dependence of the heating rate upon the loop parameters for the various heating models:

a) Acoustic mode/viscous damping:

$$E_H \propto T^2. \tag{B5}$$

b) Acoustic mode/shock wave damping:

$$E_H \propto pT^{-1/2}. \tag{B6}$$

c) Alfvén mode/anomalous conduction damping:

$$E_H \propto p^{1/2}T^{-1}. \tag{B7}$$

d) Alfvén mode/mode conversion:

$$E_H \propto p^{7/6} \propto pR^{-1}. \tag{B8}$$

b) *Coronal Current Dissipation*

An alternative method of heating the quiescent corona is by means of the anomalous dissipation of almost force-free currents induced in the corona; this possibility has been suggested by Tucker (1973) and investigated in detail by Rosner *et al.* (1978). In the present context, current dissipation is distinguished from the previous wave mode heating models primarily by the fact that the heating rate is relatively independent of the local plasma parameters once onset of anomalous dissipation is attained. Thus, there is no local heating parameter analogous to the wave damping scale length λ; instead, local heating is totally determined by the current generation rate, the latter dependent upon the rate at which turbulent fluid stresses are communicated to the magnetic field at the photospheric level. If we assume with Tucker (1973) that the rate at which the fields are stressed is proportional to the level of fluid turbulence and further assume that the base pressure is proportional to the level of fluid turbulence as well, we find that the local coronal heating rate is also simply proportional to the base pressure:

$$E_H \propto p. \tag{B9}$$

We refer the reader to the previously cited two references for the details of the current heating mechanism.

APPENDIX C

VARIATION OF TEMPERATURE ALONG A LOOP

The formalism developed in § III can also be used to generate very detailed loop models including temperature and density profiles which can be compared with observations. Our present objective is to obtain these theoretical results; detailed modeling is not attempted here. As an example, we compute the structure of a coronal loop; using equations (3.13), (3.14), and (3.16), and assuming both the pressure and heating rate to be uniform along the loop, we obtain the analytic solution

$$s(T) = s(T_0) + 2.5 \times 10^5 p^{-1}\{9.6 \times 10^{-16} T_m^3[\arcsin(T/T_m) - (T/T_m)(1 - (T/T_m)^2)^{1/2}] + 1\}, \tag{C1}$$

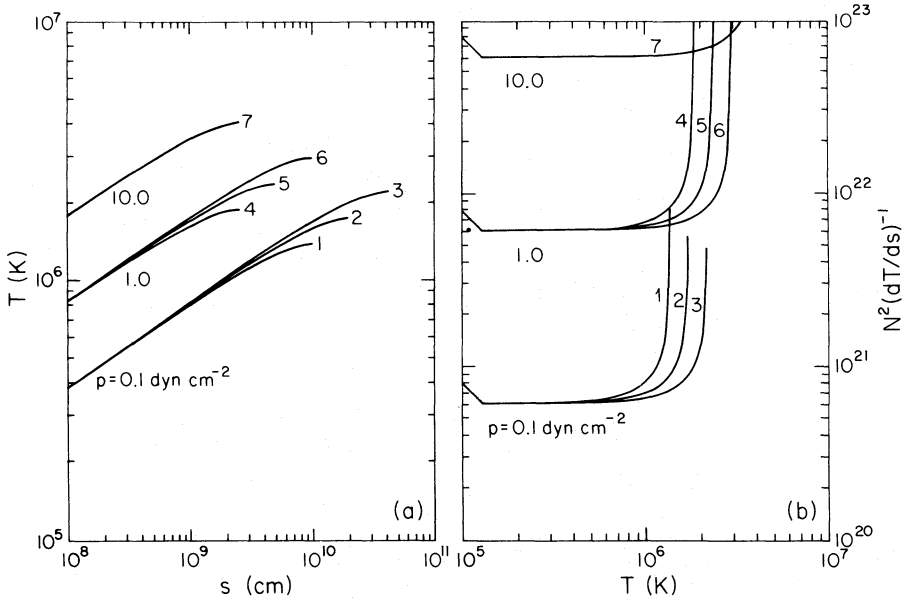

FIG. 11.—Loop atmospheres generated from the analytic model. (*a*) Temperature versus distance along loop for a variety of loop pressures (*p*) and loop sizes; (*b*) differential emission measure for loop atmospheres of Fig. 12*a*; these can be used directly to predict the expected EUV and X-ray intensities from these loops (cf. Rosner and Vaiana 1977).

where T_m is the maximum loop temperature given by equation (4.3). The inversion $T = T(s)$ cannot be obtained analytically but is easily calculated numerically; the advantage of using equation (C1) rather than direct numerical integration of the energy equation (3.4) is that it avoids problems related to large temperature gradients (e.g., the transition zone). Several loop temperature profiles for a variety of base pressure and loop sizes are shown in Figure 11*a*.

Analogously, one can analytically solve for the local conductive flux $F_c(T)$ and calculate the differential emission measure

$$\mathrm{DEM(T)} \equiv N_e^2(dT/ds)^{-1} = \frac{p^2}{4k^2}\frac{\kappa T^{1/2}}{|F_c|}. \tag{C2}$$

Thus, using equations (3.13′), (3.14), and (3.15), we obtain

$$F_c(T) \approx -2 \times 10^6 \kappa p T^{1/2}\left\{\begin{bmatrix} 10^{-10.23}T^2, & T < 10^{5.11} \\ 1, & T > 10^{5.11}\end{bmatrix} - (T/T_m)^{5/2}(1 - (T_0/T)^{7/2})\right\}^{1/2}; \tag{C3}$$

and, combining equations (C.2) and (C.3),

$$\mathrm{DEM(T)} = 6.3 \times 10^{21} p\left\{\begin{bmatrix} 10^{-10.23}T^2, & T < 10^{5.11} \\ 1, & T > 10^{5.11}\end{bmatrix} - (T/T_m)^{5/2}(1 - (T_0/T)^{7/2}\right\}^{-1/2}. \tag{C4}$$

The differential emission measure is quite useful for comparison between the models and observations because it can be used to directly compute the expected EUV line and X-ray broad-band and line emission from a given loop; a suitable procedure for choosing model parameters developed in the context of coronal hole modeling is discussed by Rosner and Vaiana (1977). The differential emission measures corresponding to the model loops shown in Figure 11*a* are displayed in Figure 11*b*.

REFERENCES

Athay, R. G. 1976, *The Solar Chromosphere and Corona: Quiet Sun* (Dordrecht: Reidel).
Braginskii, S. I. 1965, *Rev. Plasma Phys.*, **1**, 205.
Bruner, E. L., Chipman, E. G., Lites, B. W., Rottman, G. J., Shine, R. A., Athay, R. G., White, O. R. 1976, *Ap. J. (Letters)*, **210**, L97.
Cox, D., and Tucker, W. H. 1969, *Ap. J.*, **156**. 87.
Davis, J. M., Gerassimenko, M., Krieger, A. S., and Vaiana, G. S. 1975, *Solar Phys.*, **45**, 393.
De Loore, C. 1970, *Ap. Space Sci.*, **6**, 60.
Dunn, R. B. 1971, in *Physics of the Solar Corona*, ed. C. J. Macris (Dordrecht: Reidel), p. 114.
Field, G. B. 1965, *Ap. J.*, **142**, 531.
Foukal, P. V. 1976, *Ap. J.*, **210**, 575.
Gerassimenko, M., Nolte, J. T., and Petrasso, R. D. 1976, *Solar Phys.*, **48**, 121.
Gerassimenko, M., Soladyna, C. V., and Nolte, J. T. 1977, submitted to *Solar Phys.*

Jackson, J. D. 1962, *Classical Electrodynamics* (New York: Wiley).
Jordan, C. 1976, *Phil. Trans. R. Soc. London, A*, **281**, 391.
Kahler, S. 1976, *Solar Phys.*, **48**, 255.
Krieger, A. S., Chase, R. C., Gerassimenko, M., Kahler, S. W., Timothy, A. F., and Vaiana, G. S. 1975, in *IAU Symposium No. 68, Solar Gamma, X, and EUV Radiation*, ed. S. Kane (Dordrecht: Reidel), p. 103.
Krieger, A. S., Vaiana, G. S., and Van Speybroeck, L. P. 1971, in *IAU Symposium No. 43, Solar Magnetic Fields*, ed. R. Howard (Dordrecht: Reidel), p. 397.
Lamb, H. 1909, *London Math. Soc. Proc.*, **7**, 122.
Landau, L. D., and Lifshitz, E. M. 1959, *Fluid Mechanics* (London: Pergamon).
Landini, M., and Monsignori-Fossi, B. C. 1973, *Astr. Ap.*, **25**, 9.
———. 1975, *Astr. Ap.*, **42**, 213.
Landini, M., Monsignori-Fossi, B. C., Krieger, A. S., and Vaiana, G. S. 1975, *Solar Phys.*, **44**, 69.
Maxson, C. W., and Vaiana, G. S. 1977, *Ap. J.*, **215**, 919.
McIntosh, P. S., Krieger, A. S., Nolte, J. T., and Vaiana, G. S. 1976, *Solar Phys.*, **49**, 57.
McWhirter, R. W. P., Thonemann, P. C., and Wilson, R. 1975, *Astr. Ap.*, **40**, 63.
McWhirter, R. W. P., and Wilson, R. 1976, *Phil. Trans. R. Soc. London A*, **281**, 331.
Moore, R. L., and Fung, P. C. W. 1972, *Solar Phys.*, **23**, 78.
Neupert, W. M., Nakagawa, Y., and Rust, D. M. 1975, *Solar Phys.*, **43**, 359.
Pallavicini, R., Serio, S., and Vaiana, G. S. 1977, *Ap. J.*, **216**, 108.
Pallavicini, R., and Vaiana, G. S. 1976, *Solar Phys.*, **49**, 297.
Pikeln'er, S. B. 1971, *Solar Phys.*, **17**, 44.
Pneuman, G. W. 1973, *Solar Phys.*, **28**, 247.
Poletto, G., Vaiana, G. S., Zombeck, M. V., Krieger, A. S., and Timothy, A. F. 1975, *Solar Phys.*, **44**, 83.
Pottasch, S. R. 1965, *B.A.N.*, **18**, 8.
Pye, J. P., Evans, K. D., Hutcheon, R. J., Gerassimenko, M., Davis, J. M., Krieger, A. S., and Vesecky, J. F. 1977, *Astr. Ap.*, in press.
Raymond, J. 1978, in preparation.
Reeves, E. M., Timothy, J. G., Foukal, P. V., Huber, M. C. E., Noyes, R. W., Schmahl, E. J., Vernazza, J. E., and Withbroe, G. L. 1976, in *Progress in Astronautics and Aeronautics*, Vol. **48**, ed. M. Kent, E. Stuhlinger and S. T. Wu (New York: AIAA), 73.
Reidy, W. P., Vaiana, G. S., Zehnpfennig, T., and Giacconi, R. 1968, *Ap. J.*, **151**, 333.
Rosner, R., Golub, L., Coppi, B., and Vaiana, G. S. 1978, *Ap. J.*, in press.
Rosner, R., and Vaiana, G. S. 1977, *Ap. J.*, **216**, 141.
Rossi, B., and Olbert, S. 1970, *Introduction to the Physics of Space* (New York: McGraw-Hill).
Spitzer, L. 1962, *Physics of Fully Ionized Gases* (2d ed.; New York: Interscience).
Stein, R. F., and Leibacher, J. 1974, *Ann. Rev. Astr. Ap.*, **12**, 407.
Timothy, A. F., Krieger, A. S., and Vaiana, G. S. 1975, *Solar Phys.*, **42**, 135.
Tousey, R., *et al.* 1973, *Solar Phys.*, **33**, 265.
Tucker, W. H. 1973, *Ap. J.*, **186**, 285.
Tucker, W. H., and Koren, M. 1971, *Ap. J.*, **168**, 283.
Underwood, J. H., *et al.* 1976, in *Progress in Astronautics and Aeronautics*, Vol. **48**, ed. M. Kent, E. Stuhlinger, and S. T. Wu (New York: AIAA).
Vaiana, G. S., Davis, J. M., Giacconi, R., Krieger, A. S., Silk, J. K., Timothy, A. F., and Zombeck, M. 1973, *Ap. J. (Letters)*, **185**, L47.
Vaiana, G. S., Krieger, A. S., and Timothy, A. F. 1973, *Solar Phys.*, **32**, 81.
Vaiana, G. S., Krieger, A. S., Timothy, A. F., and Zombeck, M. V. 1976, *Astr. Space Sci.*, **39**, 75.
Vaiana, G. S., Reidy, W. P., Zehnpfennig, T., Van Speybroeck, L., and Giacconi, R. 1968, *Science*, **161**, 564.
Vaiana, G. S., and Tucker, W. H. 1974, in *X-Ray Astronomy*, ed. R. Giacconi and H. Gursky (Dordrecht: Reidel), p. 169.
Vaiana, G. S., Van Speybroeck, L., Zombeck, M. V., Krieger, A. S., Silk, J. K., and Timothy, A. F. 1977, *Space Sci. Instr.*, **3**, 19.
Vanbeveren, D., and De Loore, C. 1976, *Solar Phys.*, **50**, 99.
Van Speybroeck, L. P., Krieger, A. S., and Vaiana, G. S. 1970, *Nature*, **227**, 818.
Wentzel, D. G. 1974, *Solar Phys.*, **39**, 129.
Withbroe, G. L. 1975, *Solar Phys.*, **45**, 301.
———. 1976, invited presentation AGU, Washington, D.C. (April 1976).
Zel'dovich, Ya. B., and Raizer, Yu. P. 1968, *Elements of Gas Dynamics and the Classical Theory of Shock Waves* (New York: Academic Press).

R. ROSNER and G. S. VAIANA: Harvard College Observatory, 60 Garden Street, Cambridge, MA 02138
W. H. TUCKER: Smithsonian Astrophysical Observatory, 60 Garden Street, Cambridge, MA 02138